Electronic Supplementary Information (ESI) for

Conjugated polyaniline and water co-intercalating strategy boosting zinc-ion storage performances for rose-like vanadium oxide architectures

Jing Zeng,[†a] Zhonghua Zhang,[†a] Xiaosong Guo[*a] and Guicun Li[*a]

College of Materials Science and Engineering, Qingdao University of Science and Technology, Qingdao 266042, China

E-mail: guicunli@qust.edu.cn，guoxs06@126.com

Experimental section

Synthesis of the rose-like PVO architectures

Firstly, 0.18 g V_2O_5 is added to 40 mL aniline solution with a concentration of 8 mmol/L. Then, after magnetic stirring for a few minutes, the pH of the mixed solution is adjusted to about 3 by adding an appropriate amount of 0.1 mol/L HCl solution. After sonicated for 10 minutes, the mixed solution is transferred to Teflon-lined stainless-steel autoclave and maintained at 120 °C for 24h. After cooled to the room temperature, the precipitate is obtained via washing several times with deionized water and absolute ethanol. Finally, the blue black rose-like PVO architectures are obtained after dried in a vacuum oven at 60 °C for 24 h. For comparison, the annealed polyaniline-vanadium oxide at various temperatures of 200 °C, 350 °C and 450 °C (PVO-200, PVO-350 and PVO-450) are obtained by annealing with a heating rate of 5 °C min^{-1} in the air and cooled down to room temperature naturally. In addition, the V_2O_5 nanosheets are prepared by a reported method.[1] 0.36 g V_2O_5 is dissolved in 5 mL H_2O_2. After stirring for several minutes, 30 mL deionized water is added to form a mixture solution. Then the mixed solution is transferred into Teflon-lined autoclave and kept at 190 °C for 20 hours. Finally, V_2O_5 nanosheets are obtained by freeze-drying.

Materials characterization

The phase and structure of the sample are characterized by powder X-ray diffraction (XRD) with Cu K$_{\alpha}$ radiation (λ = 1.54178 Å). The morphology of the sample and electrodes are divulged using scanning electron microscope (SEM, JEOL, JSM-6700F) and high-resolution transmission electron microscope (HRTEM) with X-ray element analysis system (EDS). Fourier transformation infrared (FTIR) spectrum in the frequency range of 400−2000 cm^{-1} is obtained using a Jasco FT/IR-6100 FT spectrometer (Jasco, Germany). Raman spectrum is measured by a micro-Raman spectroscopy (Renishaw RM-1000, the excitation wavelength at 532 nm). Thermogravimetry analysis (TGA) is conducted on a MTC1000 thermal analysis system from 25 to 800 °C with a heating rate of 5 °C min^{-1} under an air atmosphere. Furthermore, the chemical states of the sample are estimated by X-ray photoelectron spectroscopy (XPS, ESCALAB 250Xi, Thermo Scientific). *Ex-situ* XRD and *ex-situ* XPS analyses are carried out during different discharge-charge states at 100 mA g^{-1} and between 0.4 and 1.6 V.

Electrochemical measurements

The active material (70 wt.%), conducting acetylene black (20 wt.%) and polyvinylidene fluoride (PVDF) (10 wt.%) are dissolved in N-methyl-2-pyrrolidinone (NMP) to form a slurry. Then the mixed slurry is spread on titanium foil current collector and dried for 12 hours in a vacuum condition at 60 °C to form the cathode. Electrochemical measurements are tested with CR2032 coin-type cells. The PVO architectures, zinc metal foil, glass fiber and 3 M Zn(CF$_3$SO$_3$)$_2$ mild aqueous solution as cathode, anode, separator and electrolyte, respectively. The zinc-ion batteries are assembled at ambient environmental conditions instead of at glove box. The rate capability, galvanostatic charge/discharge performances and cycle performance of the batteries are tested by the multichannel

battery test system (LAND-CT2001A) between 0.4 and 1.6 V versus Zn^{2+}/Zn at room temperature.

Cyclic voltammetry (CV, 0.1−1.0 mV s^{-1}) are performed at varied scan rates (0.1−1.0 mV s^{-1}), and

electrochemical impedance spectroscopy (EIS) measurements are tested with the frequency range

from 100 kHz to 0.01 Hz with an AUTOLAB electrochemical workstation at room temperature.
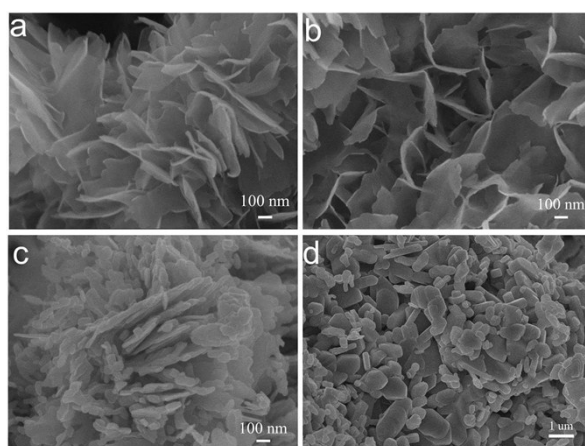

Fig. S1 SEM images of the annealed polyaniline-vanadium oxides (a) PVO-200; (b) PVO-350; (c)

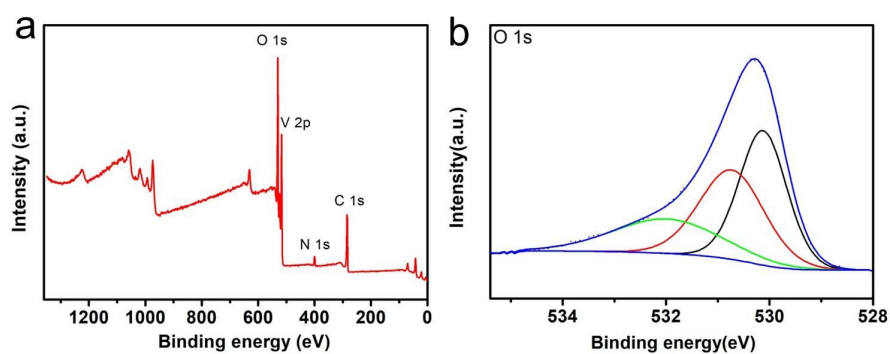PVO-450 and (d) pristine V_2O_5, respectively.

Fig. S2 The survey-scan XPS spectrum (a) of the PVO architectures; (b) O 1s XPS spectrum.
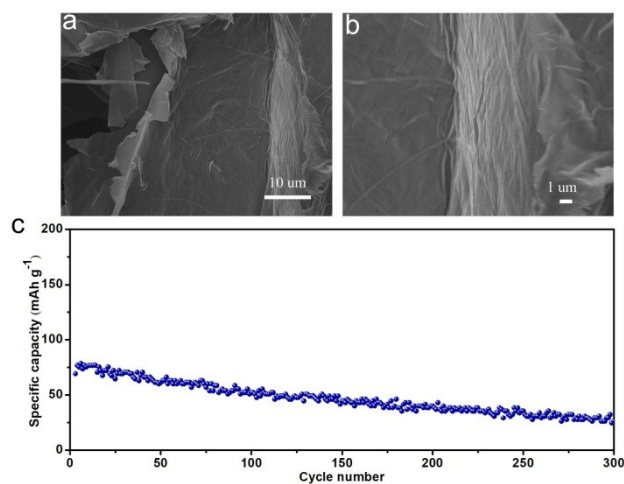
Fig. S3 (a and b) Typical SEM images of the V_2O_5 nanosheets; (c) the long cycle performance of the V_2O_5 nanosheets.
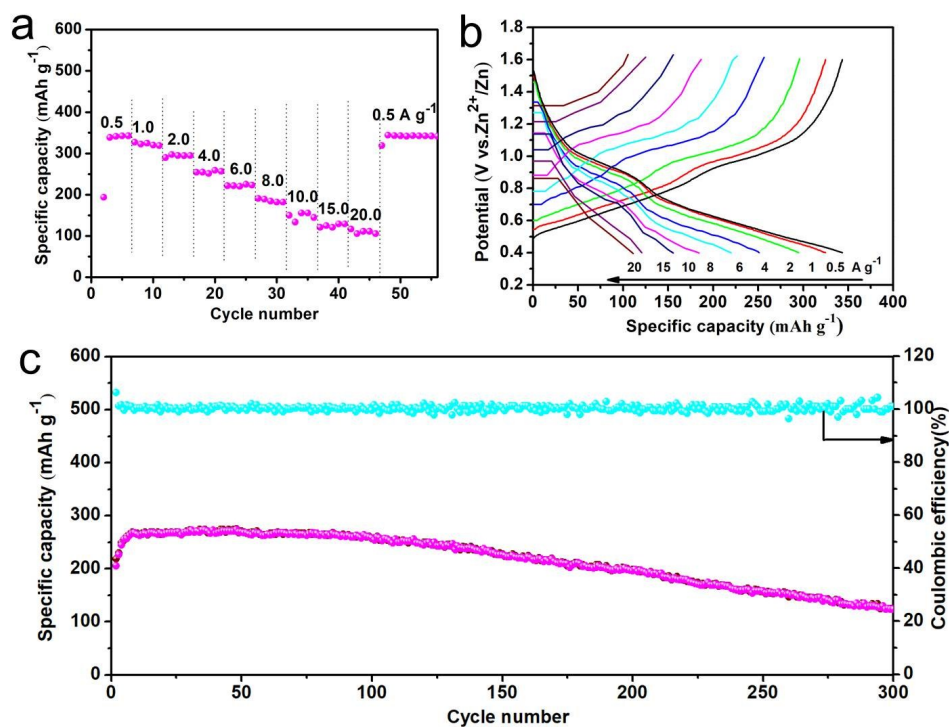

Fig. S4 (a) Rate capability and (b) discharge–charge curves at the current densities ranged from 0.5 to 20 A g^{-1}; (c) long cycle performance at 5 A g^{-1} for 300 cycles of the PVO-350.

Rate performance and the galvanostatic profile show that the discharge specific capacities are 338.4, 324.8, 294.9, 251.0, 220.0, 184.5, 155.5, 120.8 and 111.1 mAh g^{-1} at 0.5, 1.0, 2.0, 4.0, 6.0, 8.0, 10.0, 15.0 and 20.0 A g^{-1}, respectively. The long-cycle curve exhibits that the capacity retention

rate of PVO-350 electrode is about 46.6% after 300 cycles, lower than the PVO electrode.
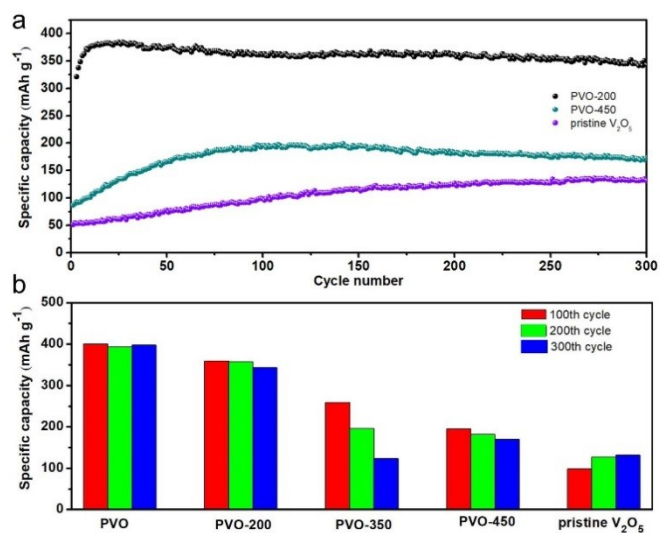

Fig. S5 (a) The long-term cycling performances of the PVO-200, PVO-450 and pristine V_2O_5 electrodes at 5 A g^{-1}. (b) The performance comparison among various electrodes at 100th cycle, 200th cycle and 300th cycle.
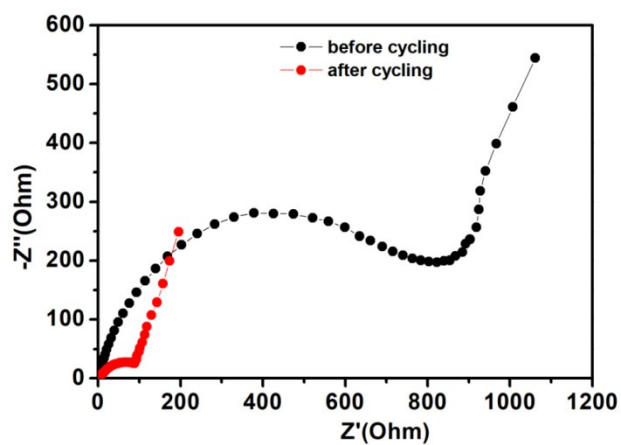

Fig. S6 Nyquist impedance plots of the PVO electrode before and after 20 cycles.
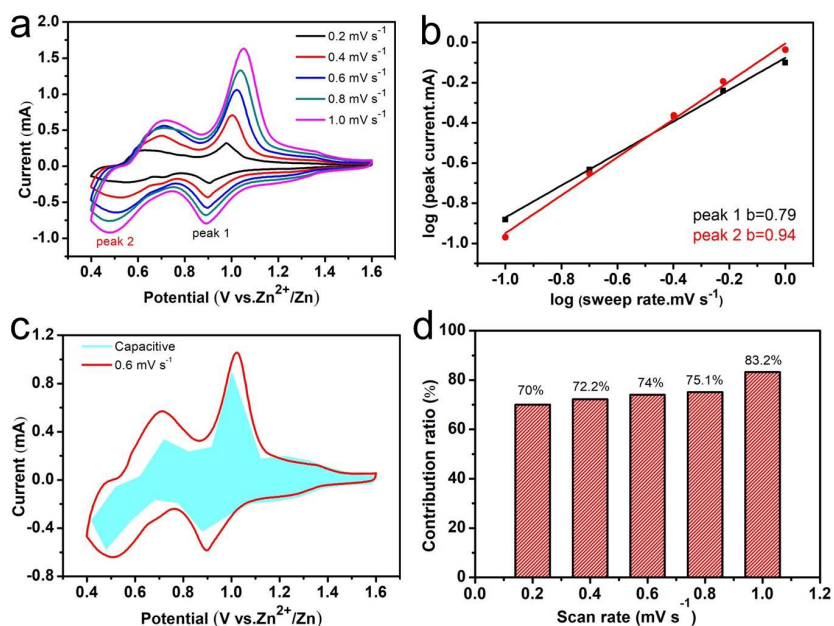
Fig. S7 (a) CV curves of the PVO electrode at various scan rates. (b) log (i) vs. log (v) plots at specific peak currents; (c) CV curve and the pseudocapacitive contribution with a scan rate of 0.6 mV s^{-1}; (d) bar chart of the percent of pseudocapacitive contribution at various scan rates.

Figure S7a presented the CV curves at various scan rates from 0.2 to 1.0 mV s^{-1} within 0.4~1.6 V, which is used to further investigate the electrochemical kinetics of the PVO electrode. Based upon the relationship between the measured peak current i (mA) and the scan rate v (mV s^{-1}), there is an equation:

$$i = av^b \tag{1}$$

This equation can be converting to:

$$log(i) = log(a)+b*log(v) \tag{2}$$

Among them, a and b are adjustable parameters. Evidently, the value of b is between 0.5 and 1.0, and when the b-value tends to 0.5 means the diffusion-limited controlled is dominating in the

electrochemical process.[2] On the other hands, when the *b*-value close to 1.0 indicated the cathode is mainly controlled by capacitive-limited process.[3] The *b*-value of the PVO electrode can be obtained by calculation and fitting the data. Figure S7b showed the *b*-values of the discharge peak 1 and peak 2 are 0.79 and 0.94. Which means that the discharge storage mainly controlled by the pseudocapacitance behavior. In order to further investigate the proportion of pseudocapacitance contribution at various scan rates, the following equations can be employed:

$$i = k_1 v^{1/2} + k_2 v \tag{3}$$

$$i/v^{1/2} = k_1 + k_2 v^{1/2} \tag{4}$$

Where the k_1 and k_2 are constants of a given potential. Meanwhile, $k_1 v^{1/2}$ represents diffusion effects and $k_2 v$ means capacitive effects. The slopes of the $v^{1/2}$ (V/s) versus $i/v^{1/2}$ (mA/(V/s)) at various potentials are presented in Figure S8. Then the pseudocapacitance contribution can be obtained by analyzing the data. Figure S7c displays the pseudocapacitance contribution at 0.6 mV s^{-1} scan rate. The red shaded area represents the pseudocapacitance contribution. While as the scan rates increases, the proportion of capacitance contribution in the electrochemical reaction gradually increases. As can be seen in Figure S7d the pseudocapacitance contribution ratios are around 70%, 72.2%, 74%, 75.1%, and 83.2% at 0.2, 0.4, 0.6, 0.8 and 1.0 mV s^{-1}, respectively. Thus, the electrochemical kinetics of the PVO electrode is mainly controlled by the capacitive-limited process. This result corresponds to fabulous rate performance of the electrode.
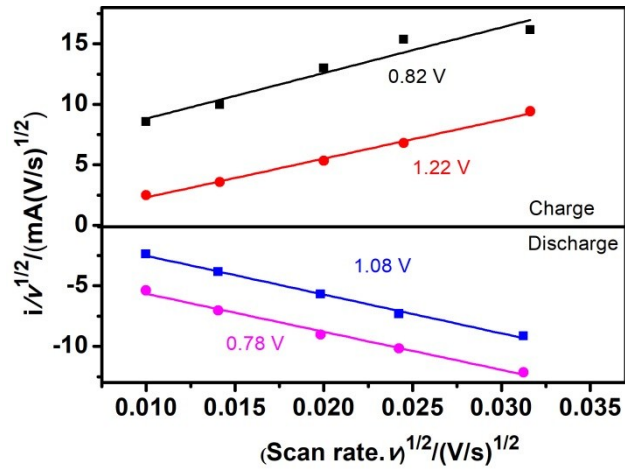
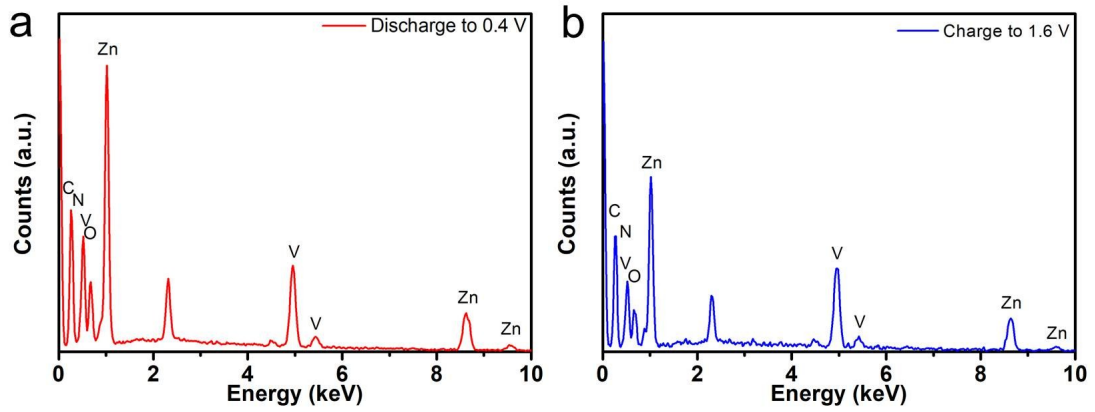**Fig. S8** i/$v^{1/2}$ versus $v^{1/2}$ plots at specific voltage.

Fig. S9 EDS spectra of the PVO electrode after discharged to 0.4 V (a) and charged to 1.6 V (b).
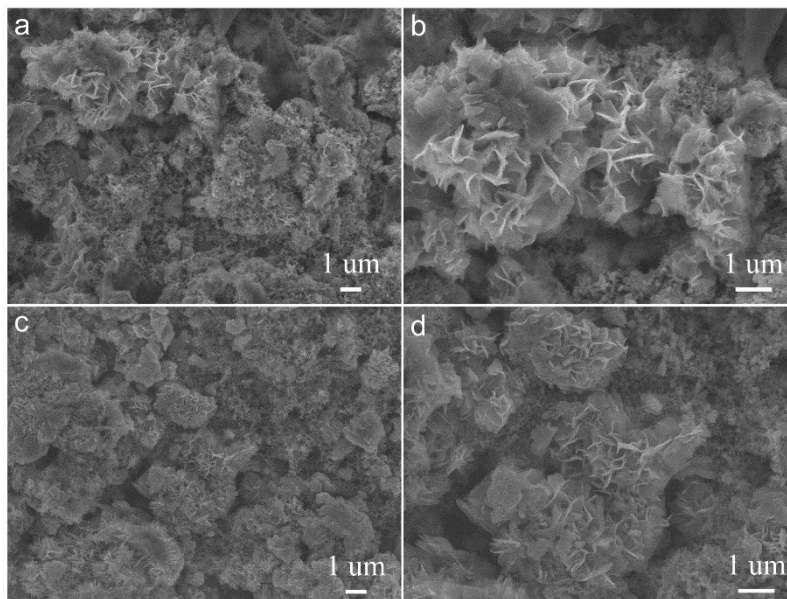

Fig. S10 SEM images of the PVO electrode (a and b) after once discharged to 0.4 V; (c and d)
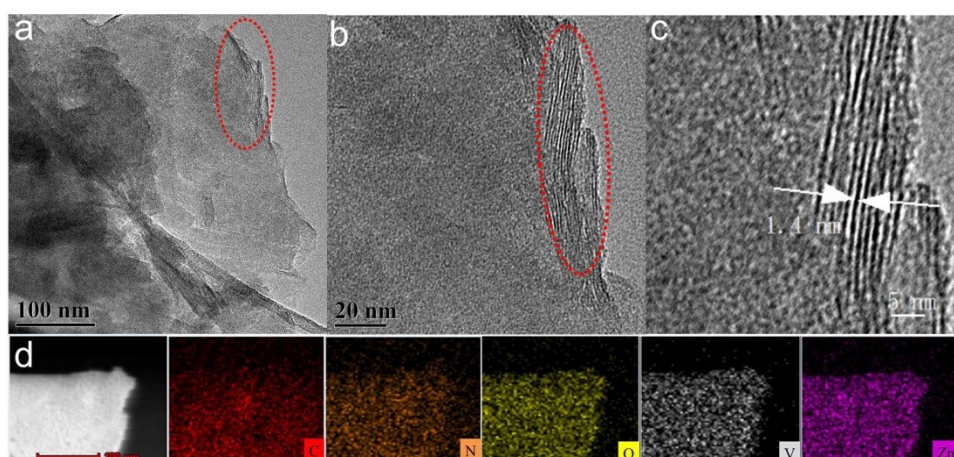
charged to 1.6 V.

Fig. S11 (a,b and c) TEM images and (d) TEM-EDS mapping images (C, N, O V and Zn elements) of the PVO electrode after discharged to 0.4 V.

Table 1 The capability performance of various reports.

Cathode material	Electrolyte	Testing voltage	Capacity
V_2O_5[4]	3 M $ZnSO_4$	0.4−1.4 V	113 mAh g^{-1} at 2.0 A g^{-1}
$V_2O_5 \cdot nH_2O$[5]	3 M $Zn(CF_3SO_3)_2$	0.2−1.6 V	372 mAh g^{-1} at 0.3 A g^{-1}
$Zn_3V_2O_7(OH) \cdot nH_2O$[6]	1 M $ZnSO_4$	0.2–1.8 V	54 mAh g^{-1} at 3.0 A g^{-1}
$Na_{0.33}V_2O_5$[7]	3 M $Zn(CF_3SO_3)_2$	0.2–1.6 V	96.4 mAh g^{-1} at 2.0 A g^{-1}
$Mg_xV_2O_5 \cdot nH_2O$[8]	3 M $Zn(CF_3SO_3)_2$	0.1–1.8 V	81 mAh g^{-1} at 5.0 A g^{-1}
$Na_2V_6O_{16} \cdot 3H_2O$[9]	1 M $ZnSO_4$	0.4–1.4 V	277 mAh g^{-1} at 3.0 A g^{-1}
$V_3O_7 \cdot H_2O$[10]	1 M $ZnSO_4$	0.5–1.8 V	275 mAh g^{-1} at 3.0 A g^{-1}
$Zn_{0.25}V_2O_5 \cdot nH_2O$[11]	1 M $ZnSO_4$	0.5–1.4 V	223 mAh g^{-1} at 4.5 A g^{-1}

$VS_4@rGO$[12]	1 M $Zn(CF_3SO_3)_2$	0.35–1.8 V	180 mAh g^{-1} at 1.0 A g^{-1}
$Li_xV_2O_5 \cdot nH_2O$[13]	2 M $ZnSO_4$	0.4-1.4 V	236 mAh g^{-1} at 5.0 A g^{-1}
Our work	3 M $Zn(CF_3SO_3)_2$	0.4−1.6 V	400 mAh g^{-1} at 5.0 A g^{-1}

References

1 J. Zhu, L. Cao, Y. Wu, Y. Gong, Z. Liu, H. E. Hoster, Y. Zhang, S. Zhang, S. Yang, Q. Yan, P. M. Ajayan and R. Vajtai, *Nano Lett.*, 2013, **13**, 5408-5413.

2 N. Zhang, Y. Dong, M. Jia, X. Bian, Y. Wang, M. Qiu, J. Xu, Y. Liu, L. Jiao and F. Cheng, *ACS Energy Lett.*, 2018, **3**, 1366-1372.

3 Y. Fang, X.-Y. Yu and X. W. Lou, *Adv. Mater.*, 2018, **30**, 1706668.

4 J. Zhou, L. Shan, Z. Wu, X. Guo, G. Fang and S. Liang, *Chem. Commun.*, 2018, **54**, 4457-4460.

5 M. Yan, P. He, Y. Chen, S. Wang, Q. Wei, K. Zhao, X. Xu, Q. An, Y. Shuang, Y. Shao, K. T. Mueller, L. Mai, J. Liu and J. Yang, *Adv. Mater.*, 2018, **30**, 1703725.

6 C. Xia, J. Guo, Y. Lei, H. Liang, C. Zhao and H. N. Alshareef, *Adv. Mater.*, 2018, **30**, 1705580.

7 P. He, G. Zhang, X. Liao, M. Yan, X. Xu, Q. An, J. Liu and L. Mai, *Adv. Energy Mater.*, 2018, **8**, 1702463.

8 F. Ming, H. Liang, Y. Lei, S. Kandambeth, M. Eddaoudi and H. N. Alshareef, *ACS Energy Lett.*, 2018, **3**, 2602-2609.

9 V. Soundharrajan, B. Sambandam, S. Kim, M. H. Alfaruqi, D. Y. Putro, J. Jo, S. Kim, V. Mathew, Y.-K. Sun and J. Kim, *Nano Lett.*, 2018, **18**, 2402-2410.

10 D. Kundu, S. Hosseini Vajargah, L. Wan, B. Adams, D. Prendergast and L. F. Nazar, *Energy Environ. Sci.*, 2018, **11**, 881-892.

11 D. Kundu, B. D. Adams, V. Duffort, S. H. Vajargah and L. F. Nazar, *Nat. Energy*, 2016, **1**, 16119.

12 H. Qin, Z. Yang, L. Chen, X. Chen and L. Wang, *J. Mater. Chem. A*, 2018, **6**, 23757-23765.

13 Y. Yang, Y. Tang, G. Fang, L. Shan, J. Guo, W. Zhang, C. Wang, L. Wang, J. Zhou and S. Liang, *Energy Environ. Sci.*, 2018, **11**, 3157-3162.